ORIGINAL ARTICLE

Folic Acid-Conjugated Fe-Au-Based Nanoparticles for Dual Detection of Breast Cancer Cells by Magnetic Resonance Imaging and Computed Tomography

Nasim Jamshidi [1], Ali Tarighatnia [2,3], Mona Fazel Ghaziyani [1*], Fakhrossadat Sajadian [1], Maryam Olad-ghaffari [1], Nader D. Nader [4]

[1] *Department of Radiology, Tabriz University of Medical Sciences, Tabriz, Iran*

[2] *Department of Medical Physics, School of Medicine, Ardabil University of Medical Sciences, Ardabil, Iran*

[3] *Research Center for Molecular and Cellular Imaging, Advanced Medical Technologies and Equipment Institute, Tehran University of Medical Sciences, Tehran, Iran*

[4] *Department of Anesthesiology, University at Buffalo, Jacobs School of Medicine and Biomedical Sciences, Buffalo, NY, USA*

*Corresponding Author: Mona Fazel Ghaziyani
Email: fazel.mona@gmail.com

Received: 07 February 2023 / Accepted: 04 March 2023

Abstract

Purpose: We synthesized folic acid-conjugated Fe_3O_4/Au-pralidoxime chloride Nanoparticles (Fe_2O_3/Au@PAM NPs) for use as dual-modal contrast agents for Magnetic Resonance Imaging (MRI) and Computed Tomography (CT) in the diagnosis of breast cancer.

Materials and Methods: Fe_2O_3/Au@PAM NPs labeled or not to folic acid were synthesized and analyzed by dynamic light scattering, transmission electron microscopy, and vibrating sample magnetometry. The ability of these NPs to create image contrast was also investigated in silico and in vitro (in MCF-7 breast cancer cells and A549 lung cancer cells) with CT and MRI.

Results: Dynamic light scattering and transmission electron microscopy revealed that the Fe_2O_3/Au@PAM NPs were nearly spherical. The average diameter of Fe_2O_3/Au NPs increased from 11.6 nm to 98 nm after folic acid conjugation. The saturation magnetization values of Fe_2O_3/Au@PAM NPs with and without folic acid conjugation were 25.56 and 32.6 emu/g, respectively. Conjugation of folic acid to NPs greatly improved their uptake by cancer cells. The additional coating of NPs with FA reduced the T2 relaxation time and signal intensity for MRI. Folic acid-labeled MCF-7 cells had a radiodensity measurement of 208 Hunsfield Units (HU) compared to 95 HU for A549 cells. For breast cancer cells, NPs labeled with folic acid significantly improved the X-ray absorption coefficient as a sign of active cellular uptake compared to NPs without labeling.

Conclusion: Folic acid-labeled Fe_2O_3/Au@PAM NPs can serve as dual CT/MRI contrast agents and improve the sensitivities of both modalities for the detection of cancer cells.

Keywords: Breast Cancer; Computed Tomography; Magnetic Resonance Imaging; Targeted Imaging.

DOI:

1. Introduction

The ability to accurately diagnose a variety of diseases has been aided by advances in molecular imaging and the development of targeted probes [1]. Such probes can reveal cellular or molecular lesions and increase treatment accuracy [2, 3]. To be successful, these probes must (i) have significant detection capability, (ii) be able to assemble in the desired targeted area, and (iii) be biocompatible [4, 5]. Diagnostic probes that use nanoparticles (NPs) as contrast agents can target tumors to enhance the detection of cancers [6], which afflict 10 million people annually according to the World Health Organization.

Breast cancer is detected by screening tests, and diagnostic modalities are then used for more detailed evaluations. For example, mammography, ultrasound, thermography, magnetic resonance imaging (MRI), Computed Tomography (CT), positron emission tomography, optical imaging, and electrical impedance imaging are used to diagnose malignant and metastatic breast cancers. Combinatorial methods provide greater anatomical and functional detail to aid clinicians in determining the degree of malignancy [7-9]. Thus, dual-modality targeted NPs have emerged as contrast agents to detect and diagnose malignant cancers at early stages [10, 11].

In previous studies, iron-based nanoparticles have been used as a negative MRI contrast agent and, in combination with other materials, as theranostic agents for cancer detection and treatment. On the other hand, gold-based nanoparticles have been employed as CT scan contrast material due to their strong X-ray attenuation coefficient [12-14].

Different NP structures have been examined for contrast enhancement of CT or dual-modal CT/MRI [10, 15]. In the present study, new NPs based on iron and gold were synthesized with folic acid with a specific coating and dendrimer structure targeting breast cancer. Due to high biocompatibility, size-tunable, and monodispersity, this structure can potentially increase the possibility of further labeling with folic acid and enhance the targeting rate in cancer diagnosis. To our knowledge, such a construct has not been studied for breast cancer detection. This evaluation has been done using CT and MRI scanners at the silico and cellular level, so if successful, it will provide the base for in vivo experiments [16]. For this purpose, we used NPs with a dendrimeric structure (polyamidoamine [PAM] dendrimers) and conjugate to FA [17].

2. Materials and Methods

2.1. Synthesis of NPs

2.1.1. Gold (Au) Dendrimer NPs

Au NPs within a PAM dendrimer were synthesized with reducing sodium borohydride ($NaBH_4$) at a ratio of 1 dendrimer to 50 Au atoms. Chloroacetic acid solution ($ClCH_2COOH$) (2.5 mL in a 2:1 water-methanol solution [v/v]) was added to PAM dendrimers in distilled water (20 mg, 10 mL) and stirred vigorously. After 30 mins, cold $NaBH_4$ solution (5 mL in in a 2:1 water-methanol solution [v/v]) was gently added to the stirring Au-salt/dendrimer mixture. The resulting mixture was dialyzed with water for 1 day using a 2000 dialysis bag (six times, 1 liter) to remove residual reagents. The final Au NPs were lyophilized.

2.1.2. Fe_3O_4 NPs

Fe(II) and Fe(III) ions were coprecipitated by adding 25 mL of a solution containing 1 M $FeCl_3{\cdot}6H_2O$, 0.5 M $FeCl_2{\cdot}4H_2O$, and 0.4 M HCl to 50 mL of 1 mM sodium hydroxide solution. The mixture was stirred at room temperature for 2 h. The resulting magnetic NPs were centrifuged at 5,000 rpm, collected, and washed with absolute ethanol. Centrifugation was performed twice, and the sediment containing the NPs was stored at 4 °C for later use.

2.1.3. Dual-Modality NPs (Fe_2O_3/Au@PAM)

Saline phosphate buffer solutions (PBS) containing 10 g of Fe_3O_4 NPs and 50 mg of Au dendrimers were mixed with stirring for 12 h. The NP mixture was dialyzed with water for 6 h using a 2-L dialysis-grade bag (three times, 300 mL) to remove the unreacted material. The final composition of Fe_2O_3/Au@PAM NPs was lyophilized and stored at 4 °C until it was used.

2.1.4. Surface Modification Fe_2O_3/Au@PAM NPs with Folic Acid

The assortment of folic acid and its conjugation on the Fe_2O_3/Au@PAM NPs surface was prepared

according to the protocol of Khademi *et al.* The mixture was stirred for 4 h at room temperature to acquire FA-labeled-NPs. Finally, the prepared labeled-NPs were purified by centrifugation and double re-precipitation from distilled water [14].

2.2. Characterization Techniques

A Philips EM208S instrument was used to record Transmission Electron Microscopy (TEM) images at 100 kV. The hydrodynamic sizing of the constructed Fe_2O_3/Au@PAM NPs was conducted by dynamic light scattering. NPs were dispersed in water and analyzed using the zeta potential analyzer Zetasizer (Nano ZS System; Malvern, UK). UV-Vis spectra of NPs were measured with a Specord 250 spectrometer (Analytik Jena AG, Germany). Samples were dispersed in water before measurements. A vibrating sample magnetometer (LBKFB model, Meghnatis Daghigh Kavir Company, Kashan, Iran) was used to measure the magnetic properties of the NPs.

2.3. Cell Cultures and Cytotoxic Assay

MCF-7 breast cancer cells and A549 lung cancer cells were cultured in RPMI 1640 medium (Biosera, Labtech International Ltd., East Sussex, UK) containing fetal bovine serum, 100 U/mL penicillin, and 10 µg/mL streptomycin at 37 °C in an atmosphere of 5% CO_2 and 95% humidified air.

Cell viability upon treatment with non-labeled or FA-labeled Fe_2O_3/Au@PAM NPs was assessed with an MTT [3-(4,5-dimethylthiazol-2-yl)-2,5-diphenyltetrazolium bromide] viability assay. A 96-well plate was seeded with 5,000 cells/well, and the cells were allowed to attach to the plate overnight. The next day, the cells were incubated for different time periods with fresh medium containing NPs. The cells were then incubated for 4 h with a fresh solution containing 0.1 g/mL MTT. The remaining insoluble formazan crystals were dissolved in isopropanol, and the absorbance was measured at 570 nm in a microplate reader. Assays were carried out in triplicates. The half maximum inhibitory concentration relevant to the labeled and non-labeled NPs was obtained 24 h and 48 h time.

2.4. In silico MRI and CT Protocol

Different concentrations of Fe_2O_3/Au@PAM NPs were prepared and transferred to the microtubes. Before imaging, MRI and CT scan systems were evaluated and calibrated for accuracy and repeatability. Then imaging was done according to the following protocols.

A clinical 1.5 T MRI scanner (MAGNETOM Avanto, Siemens Healthcare, Germany) was used for MRI and to assess the transverse relaxation rate (r2). The T2-weighted images were obtained according to a previous study [18]: repetition time, 3,000 ms; time of echo, total of 16 from 22 ms to 352 ms; flip angle, 90°; average = 3, field of view, 150 by 150 mm; resolution, 256 by 256 pixels; slice thickness, 4 mm. According to the previous method [13], similar Regions Of Interest (ROI) with identical size and position were drawn on each sample with ImageJ software. R2 values were calculated. Then a linear curve was drawn as R2 against Fe concentration, and the slope of the curve was reported as r2 relaxivity." CT scans were performed using a 128-slice GE Light Speed VCT imaging system (GE Medical Systems) with 80 kV, 200 mAs, and a slice thickness of 0.625 mm. The prepared NPs were dispersed in water with different Au concentrations (0.31, 0.62, 1.25, 2.5, and 10 mM). Samples were placed in 1.5-mL Eppendorf tubes in a self-designed scanning holder.

Contrast enhancement was evaluated by loading the DICOM format CT and MRI files into ImageJ software and selecting a uniformly sized round region of interest for each sample.

2.5. In Vitro MRI/CT

MCF-7 and A549 cells (2.5 ×106 cells) were incubated for 4 h with 100 µM FA-labeled NPs or 100 µM non-labeled NPs at 37 ℃ and 5% CO_2. In addition, MCF-7 cells were incubated with 0.1, 0.05, and 0.025 mM of Fe and 10, 5, and 2.5 mM of gold. The cells were then washed with PBS three times, lysed with trypsin, centrifuged, and resuspended in 1 mL PBS (containing 1% agarose) in a 1.5-mL Eppendorf tube. Cross-section T2-weighted MRI and CT images of the cell suspension in each sample tube were performed using both modalities; then, the ROI was determined

as described above in section 2.4. Their MSI and HU were calculated with ImageJ software.

2.6. Statistical Analysis and Data Management

The Kolmogorov-Smirnov test was used to determine if the data were normally distributed. The means (± standard deviations) were analyzed with mean comparison tests, factor analyses of variance, and chi-square tests by using SPSS 27 software (IBM-SPSS Statistics, Chicago, IL) and Prism 8.0 (Graph Pad Software, San Diego, CA). P values of <0.05 were considered statistically significant.

3. Results

3.1. Characterization of FA-Conjugated Fe_2O_3/Au@PAM NPs

Non-labeled Fe_2O_3/Au@PAM NPs were nearly spherical, with a mean diameter of 11.6 ± 3.8 nm (Figure 1A). The hydrodynamic diameter of Fe_2O_3/Au@PAM NPs was measured by dynamic light scattering (Figure 1B). Figure 1C shows the UV-Vis absorption spectra of the prepared NPs. Two peaks were seen in the range of 200 nm to 300 nm, representing the dendrimer and iron oxide, respectively. In addition, the peak at 500 nm was related to the Au.

The magnetic hysteresis loops of the FA-labeled and non-labeled Fe_2O_3/Au@PAM NPs at room temperature are depicted in Figure 1D. The plot represents the magnetization "M" versus the applied field "H" (between −9 and +9 kilooersted [kOe]) of the prepared NPs. The saturation magnetization was 25.58 emu/g for FA-labeled and 32.6 emu/g for non-labeled Fe_2O_3/Au@PAM NPs.

The viability of lung (A549) and breast (MCF-7) cancer cells exposed to labeled and non-labeled NPs was evaluated using the MTT assay. The cytotoxicity of targeted (FA-labeled) and non-targeted (non-labeled) NPs is shown in Figure 2. The viabilities of MCF-7 cells and A549 cells were similar. However, a high concentration of FA-labeled NPs was cytotoxic to MCF-7 cells. The cytotoxic effects of synthesized targeted and non-targeted nanoparticles on A459 and MCF-7 cell lines were the same at similar concentrations. More importantly, despite the expectation over 24 hours to 48 hours, a slight change in viability was not statistically significant.

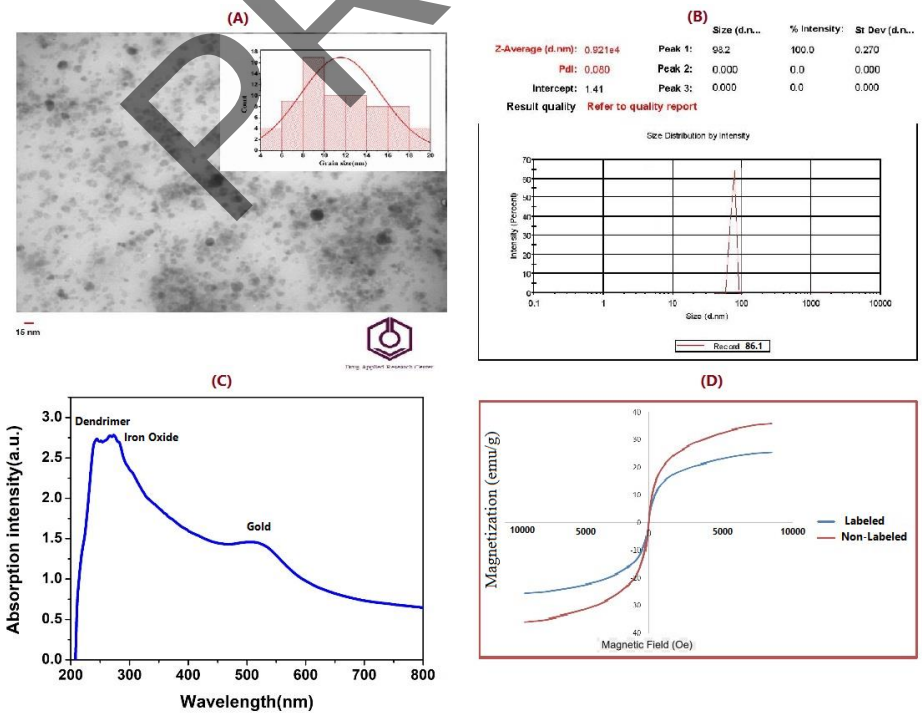

Figure 1. (A) Transmission electron microscopy image of folic acid (FA)-labeled Fe_2O_3/Au@PAM nanoparticles (NPs). (B) Dynamic light scattering analysis of NPs. (C) UV-Vis spectra of NPs. (D) Vibrating sample magnetometry FA-labeled and non-labeled NPs

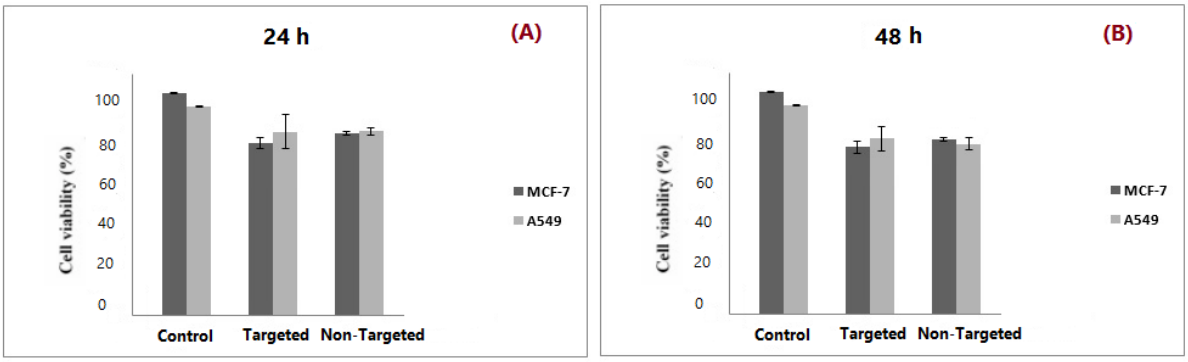

Figure 2. MTT assay results from MCF-7 and A459 cancer cells 24 h (A) and 48 h (B) after treatment with folic acid (FA)-labeled and non-labeled Fe_2O_3/Au@PAM nanoparticles (NPs)

3.2. Relaxivity Measurements and X-Ray Attenuation

Aqueous solutions of Fe_2O_3/Au@PAM NPs at different concentrations were imaged in a 1.5 T magnetic field. The transverse relaxation rate per millimolar iron (r2) was calculated. The r2 relaxivity values were 162 mM-1 s-1 for Fe_2O_3/Au@PAM NPs but 245 mM-1 s-1 for other iron NPs with the same iron concentration (Figure 3A). This difference was associated with decreases in T2 signal intensity that were more pronounced in samples of Fe_3O_4 NPs.

Figure 3B shows X-ray attenuation with increasing Au concentrations. This contrast change was more evident in the hybrid (Fe_2O_3/Au@PAM) NPs than in Au-only NPs. NPs with an Au concentration of 10 mM have the highest Hounsfield unit (HU) values as shown in the relevant figure.

3.3. In Vitro Targeted Dual-Modal CT/MRI of Cancer Cells

MRI revealed marked signal differences (Figure 4A). a mean signal intensity (MSI) was dramatically lower for cells incubated with FA-labeled Fe_2O_3/Au@PAM NPs (0.1 mM): 546 lower for MCF-7 cells ($P < 0.001$), and 260 lower for A549 cells ($P > 0.05$). Furthermore, the signal intensity on a T2-weighted MR image in MCF-7 cells increased to 1,062 when the iron concentration was decreased to 0.025 mM, suggesting an inverse correlation between MSI and the concentration of iron in NPs.

A quantitative analysis determined the difference in brightness between the examined cells. The X-ray attenuation (expressed as HU) for cells labeled with Fe_2O_3/Au@PAM NPs was 208 HU for MCF-7 cells and 95 HU for A549 cells, which was much higher than for non-labeled cells (Figure 4B).

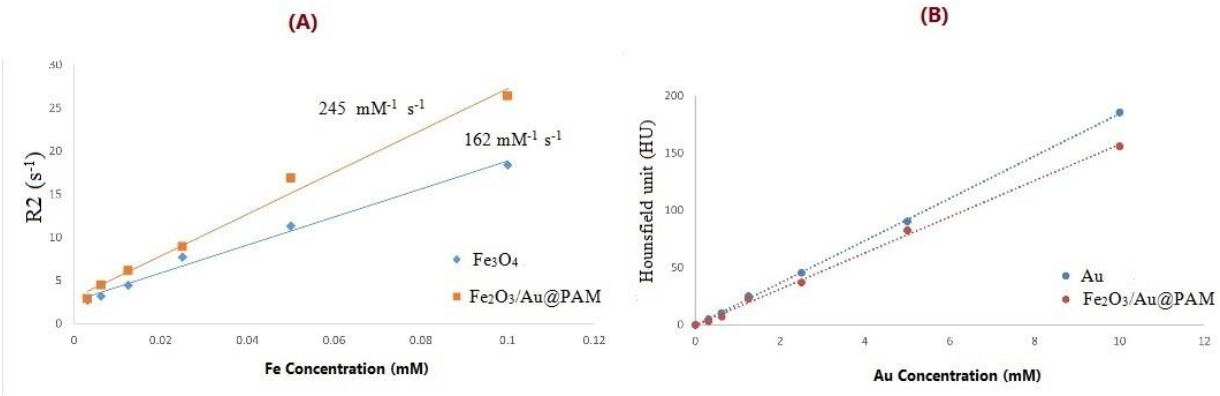

Figure 3. (A) Quantitative analysis of r2 from MRI of Fe-containing nanoparticles (NPs) and NPs with different Au concentrations. (B) The relationship between concentration and Hounsfield unit (HU) values for Au NPs and Fe_2O_3/Au NPs

The increased brightness depended on Au concentration as an active element.

The results demonstrate that FA conjugation enhanced the contrast of cancer cells in CT imaging and MRI.

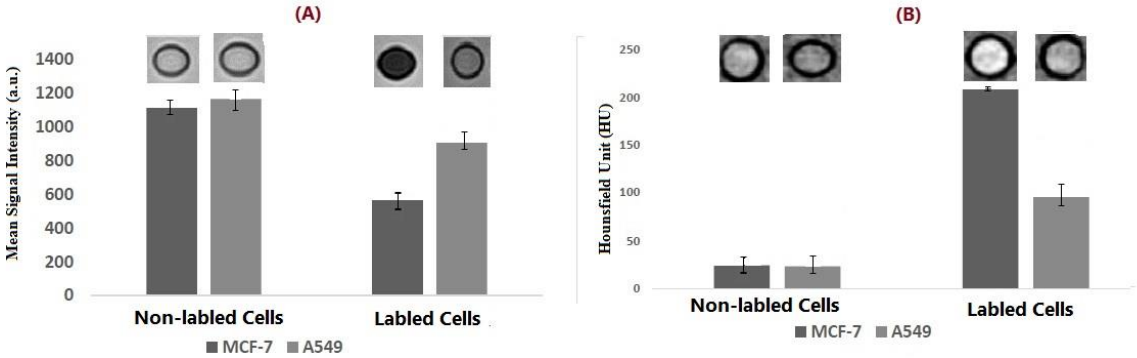

Figure 4. A) MRI images and quantitative analysis of non-labeled and labeled A459 and MCF-7 cell lines; (B) CT images and quantitative analysis of the two cell lines mentioned in the conjugation with Fe3O4/Au@PAM and Fe3O4/Au@PAM-FA

4. Discussion

From a clinical point of view, CT is a fast technique with the ability to show the bony, air, and metastatic structures of tissues and tumors. Meanwhile, MRI is the standard gold method in the anatomical representation of tissue. Compared to MRI, CT scanning provides better spatial resolution but lower contrast resolution. However, the weaknesses of each imaging technique can be offset by combining these modalities to improve the accuracy of disease diagnosis. To apply this to the detection and diagnosis of cancers, a dual-modality contrast agent is needed. Here, we describe the synthesis of a CT/MRI NP that enhances the imaging contrast for cancer cells, particularly breast cancer cells. Our analyses revealed that the dual Fe_2O_3/Au@PAM NPs increase X-ray attenuation and decrease the recovery rate and T2 relaxation time when imaging cancer cells. Therefore, we were able to improve the signal for both imaging modalities.

There are two crucial factors for targeting high-performance NPs to tumors: surface functionalization and size control [19]. The constructed NPs were nearly spherical in structure, but the conjugation of FA introduced some irregularities to the surfaces of the NPs. Nevertheless, the spherical morphology of the NPs was maintained [20]. The size of the NPs we synthesized should not impede their blood circulation time or the amount of accumulation in targeted (i.e., tumor) tissues.

In addition, the polydispersity index of Fe_2O_3/Au@PAM NPs was 0.080. The smaller size of the NPs determined from transmission electron microscopy relative to that from dynamic light scattering (11 nm vs. 98 nm, respectively) may reflect the measurement of single particles in a dried state versus that of particle clusters in an aqueous solution [5, 16, 21].

The magnetometry result indicated that the NPs are reactive to magnetic fields. The data also suggest that the surface conjugation of FA lowers the saturation magnetization values of NPs. Because the NPs did not maintain magnetization when exposed to a peripheral magnetic field, they represent an ideal MRI contrast agent for cancer detection. In addition, the negligible hysteresis of NPs suggests that they have superparamagnetic characterization at room temperature [22].

FA labeling to target cancer cells did not alter the cytotoxicity of nanoparticles. Changing the time from 24 hours to 48 hours did not significantly induce higher cytotoxicity. However, prolonged exposure may lead to cell death, especially for MCF-7 cells. Dephasing of transverse magnetization and reduction of the value of transverse relaxation time (T2) have been associated with Fe-based NPs, which are often used as a T2 negative contrast agent and reduce the MR signal [23, 24]. The r2 relaxation reduction of dual Fe_2O_3/Au NPs is due to their multilayer coating that shields the surfaces of NPs from water molecules. The r2 relaxivity was reduced to 162 mM−1 s−1 vs. the 71.55 mM-1s-1 reported in the study

by Cai *et al.* [25]. The difference may be attributable to the different methods of synthesis, as in the present study, Au NPs were first attached to the dendrimer and then coated with Fe_3O_4. Furthermore, the r2 of the Fe_2O_3/Au@PAM NPs was much higher in the study by Cai *et al.* [25] than in our results (245 mM^{-1} s^{-1} vs. 162.27 mM^{-1} s^{-1}, respectively). The authors of that study explained that multiple small magnets could effectively influence the water molecules in their vicinity in their synthesized compound because of the synergistic effect when more than one Fe NP is attached to each Au NP [25]. Their analysis of MRI and CT images confirmed that Fe_3O_4/Au@PAM NPs produce image contrast for dual-modal imaging applications. Our imaging analyses of cancer cells revealed that cellular uptake of the Fe_2O_3/Au@PAM NPs explicitly hampered the MR, consistent with the results of the study by Cai *et al.* [25].

5. Conclusion

The findings presented here demonstrate the feasibility and efficacy of the dual-modality NPs as contrast agents for cancer detection in vitro. Specifically, FA-labeled Fe_2O_3/Au@PAM NPs target cancer cells for detection by MRI and CT. Importantly; these NPs show low toxicity and cellular uptake by breast cancer as a result of FA receptor-mediated endocytosis, which can facilitate the identification of breast cancer cells at an early stage. Further research and field investigations are needed to evaluate the stability and potential toxicity of these NPs in an in vivo environment and to assess blood circulation after intravenous administration in mice.

Acknowledgments

Funding was provided by Tabriz University of Medical Sciences.

This study was reviewed and approved by the Ethical Committee of Tabriz University of Medical Sciences [IR.TBZMED.VCR.REC.1399.137].

References

1- Ali Tarighatnia, Gurkaran Johal, Ayuob Aghanejad, Hossein Ghadiri, and Nader D Nader, "Tips and Tricks in Molecular Imaging." *Frontiers in Biomedical Technologies*, Vol. 8 (No. 3), pp. 226-35, (2021).

2- E. A. Schellenberger, F. Reynolds, R. Weissleder, and L. Josephson, "Surface-functionalized nanoparticle library yields probes for apoptotic cells." (in eng), *ChemBioChem*, Vol. 5 (No. 3), pp. 275-9, Mar 5 (2004).

3- F. A. Jaffer and R. Weissleder, "Seeing within: molecular imaging of the cardiovascular system." (in eng), *Circ Res*, Vol. 94 (No. 4), pp. 433-45, Mar 5 (2004).

4- Nguyen Viet Long, Yong Yang, Toshiharu Teranishi, Cao Thi, Yanqin Cao, and M. Nogami, "Biomedical Applications of Advanced Multifunctional Magnetic Nanoparticles." *Journal of Nanoscience and Nanotechnology*, Vol. 15pp. 1-17, 12/01 (2015).

5- Rajkumar S and Prabaharan M, "Multi-functional core-shell Fe3O4@Au nanoparticles for cancer diagnosis and therapy." *Colloids and Surfaces B: Biointerfaces*, Vol. 174pp. 252-59, 2019/02/01/ (2019).

6- Sh Karamipour, M. S. Sadjadi, and N. Farhadyar, "Fabrication and spectroscopic studies of folic acid-conjugated Fe3O4@Au core-shell for targeted drug delivery application." (in eng), *Spectrochim Acta A Mol Biomol Spectrosc*, Vol. 148pp. 146-55, Sep 5 (2015).

7- Mohammad Madani, Mohammad Mahdi Behzadi, and Sheida Nabavi, "The role of deep learning in advancing breast cancer detection using different imaging modalities: A systematic review." *Cancers*, Vol. 14 (No. 21), p. 5334, (2022).

8- Md Shafiul Islam, Naima Kaabouch, and Wen Chen Hu, "A survey of medical imaging techniques used for breast cancer detection." in *IEEE International Conference on Electro-Information Technology, EIT 2013*, (2013): *IEEE*, pp. 1-5.

9- Jamileh Kadkhoda, Ali Tarighatnia, Mohammad Reza Tohidkia, Nader D Nader, and Ayuob Aghanejad, "Photothermal therapy-mediated autophagy in breast cancer treatment: Progress and trends." *Life Sciences*, p. 120499, (2022).

10- Shang-Wei Chou, Yu-Hong Shau, Ping-Ching Wu, Yu-Sang Yang, Dar-Bin Shieh, and Chia-Chun Chen, "In vitro and in vivo studies of FePt nanoparticles for dual modal CT/MRI molecular imaging." *Journal of the American Chemical Society*, Vol. 132 (No. 38), pp. 13270-78, (2010).

11- Ali Tarighatnia *et al.*, "Mucin-16 Targeted Mesoporous Nano-system for Evaluation of Cervical cancer via Dual-modal Computed Tomography and Ultrasonography." *New Journal of Chemistry*, 10.1039/D1NJ04123A (2021).

12- Anita Ebrahimpour *et al.*, "Detection of glioblastoma multiforme using quantitative molecular magnetic resonance imaging based on 5-aminolevulinic acid: in vitro and in vivo studies." *Magnetic Resonance Materials in Physics, Biology and Medicine*, pp. 1-13, (2022).

13- Anita Ebrahimpour *et al.*, "Magnetic Metal–Organic Framework Based on Zinc and 5-Aminolevulinic Acid: MR Imaging and Brain Tumor Therapy." *Journal of Inorganic and Organometallic Polymers and Materials*, Vol. 31pp. 1208-16, (2021).

14- Sara Khademi *et al.*, "Folic acid-cysteamine modified gold nanoparticle as a nanoprobe for targeted computed tomography imaging of cancer cells." *Materials Science and Engineering: C*, Vol. 89pp. 182-93, (2018).

15- Ali Tarighatnia *et al.*, "Engineering and quantification of bismuth nanoparticles as targeted contrast agent for computed tomography imaging in cellular and animal models." *Journal of drug delivery science and technology*, Vol. 66p. 102895, (2021).

16- N. Kohler, C. Sun, J. Wang, and M. Zhang, "Methotrexate-modified superparamagnetic nanoparticles and their intracellular uptake into human cancer cells." (in eng), *Langmuir*, Vol. 21 (No. 19), pp. 8858-64, Sep 13 (2005).

17- Shewaye Lakew Mekuria, Tilahun Ayane Debele, and Hsieh-Chih Tsai, "PAMAM dendrimer based targeted nano-carrier for bio-imaging and therapeutic agents." *RSC Advances*, 10.1039/C6RA12895E Vol. 6 (No. 68), pp. 63761-72, (2016).

18- Seraj Mohaghegh, Ali Tarighatnia, Yadollah Omidi, Jaleh Barar, Ayuob Aghanejad, and Khosro Adibkia, "Multifunctional magnetic nanoparticles for MRI-guided co-delivery of erlotinib and L-asparaginase to ovarian cancer." *Journal of Microencapsulation*, Vol. 39 (No. 4), pp. 394-408, (2022).

19- F. M. Sirotnak and B. Tolner, "Carrier-mediated membrane transport of folates in mammalian cells." (in eng), *Annu Rev Nutr*, Vol. 19pp. 91-122, (1999).

20- Sergio Andrés Torres-Pérez, María del Pilar Ramos-Godínez, and Eva Ramón-Gallegos, "Effect of methotrexate conjugated PAMAM dendrimers on the viability of breast cancer cells." *AIP Conference Proceedings*, Vol. 2090 (No. 1), p. 050014, 2019/04/10 (2019).

21- Hongdong Cai *et al.*, "Dendrimer-Assisted Formation of Fe3O4/Au Nanocomposite Particles for Targeted Dual Mode CT/MR Imaging of Tumors." *Small*, https://doi.org/10.1002/smll.201500856 Vol. 11 (No. 35), pp. 4584-93, 2015/09/01 (2015).

22- Limin Guo *et al.*, "Hollow mesoporous carbon spheres—an excellent bilirubin adsorbent." *Chemical Communications*, 10.1039/B911083F (No. 40), pp. 6071-73, (2009).

23- Heyu Yang *et al.*, "Effects of iron oxide nanoparticles as T2-MRI contrast agents on reproductive system in male mice." *Journal of Nanobiotechnology*, Vol. 20 (No. 1), p. 98, 2022/03/02 (2022).

24- Chen Bai *et al.*, "Synthesis of Ultrasmall Fe3O4 Nanoparticles as T1–T2 Dual-Modal Magnetic Resonance Imaging Contrast Agents in Rabbit Hepatic Tumors." *ACS Applied Nano Materials*, Vol. 3 (No. 4), pp. 3585-95, 2020/04/24 (2020).

25- Hongdong Cai *et al.*, "Facile assembly of Fe3O4@Au nanocomposite particles for dual mode magnetic resonance and computed tomography imaging applications." *Journal of Materials Chemistry*, 10.1039/C2JM16851K Vol. 22 (No. 30), pp. 15110-20, (2012).